



University of Warwick institutional repository: <http://go.warwick.ac.uk/wrap>

This paper is made available online in accordance with publisher policies. Please scroll down to view the document itself. Please refer to the repository record for this item and our policy information available from the repository home page for further information.

To see the final version of this paper please visit the publisher's website. Access to the published version may require a subscription.

Author(s): J. Liu, R.J. Chater, B. Hagenhoff, R.J.H. Morris and S.J. Skinner,

Article Title: Surface enhancement of oxygen exchange and diffusion in the ionic conductor $\text{La}_2\text{Mo}_2\text{O}_9$

Year of publication: 2010

Link to published article: <http://dx.doi.org/10.1016/j.ssi.2010.04.009>

Publisher statement: NOTICE: this is the author's version of a work that was accepted for publication in Solid State Ionics. Changes resulting from the publishing process, such as peer review, editing, corrections, structural formatting, and other quality control mechanisms may not be reflected in this document. Changes may have been made to this work since it was submitted for publication. A definitive version was subsequently published in Solid State Ionics, Vol. 181, Issue 17-18, 17th June 2010, DOI: 10.1016/j.ssi.2010.04.009

Surface Enhancement of Oxygen Exchange and Diffusion in the Ionic Conductor $\text{La}_2\text{Mo}_2\text{O}_9$

J. Liu ^a, R. J. Chater ^a, B. Hagenhoff ^b, R. J. H. Morris ^c, S. J. Skinner ^{a, *}

^a *Department of Materials, Imperial College London, Prince Consort Road, London SW7 2BP, UK*

^b *TASCON GmbH, Heisenbergstr.15, D-48149 Münster, Germany*

^c *Department of Physics, University of Warwick, Gibbet Hill Road, Coventry, CV4 7AL, UK*

Abstract

Isotopic surface oxygen exchange and its subsequent diffusion has been measured using secondary ion mass spectrometry in the fast ionic conductor $\text{La}_2\text{Mo}_2\text{O}_9$. A silver coating was applied to the sample surface to enhance the surface exchange process for dry oxygen. Contrary to previous studies performed using a wet atmosphere, no grain boundary diffusion tail was observed under these optimized dry exchange conditions. The activation energy for oxygen diffusion was found to be $0.66(\pm 0.09)$ eV at high temperature ($>570^\circ\text{C}$), and $1.25(\pm 0.01)$ eV at low temperature ($<570^\circ\text{C}$). Time-of-Flight secondary ion mass spectrometry was employed to investigate the correlation between the silver coating and the ^{18}O concentration on the sample surface. A close correlation between the presence of silver and oxygen incorporation on the surface was observed.

Keywords: $\text{La}_2\text{Mo}_2\text{O}_9$; Oxygen diffusion; Surface exchange; Silver

* Corresponding author. Stephen J. Skinner, Department of Materials, Imperial College London, Prince Consort Road, London SW7 2BP, UK. Tel: +44 (0)20 7594 6782 Fax: +44 (0)20 7594 6757

Email address: s.skinner@imperial.ac.uk

1. Introduction

Fast oxide-ion conductors have been attracting considerable attention because of their wide range of applications, some of which include the electrolyte for solid oxide fuel cells (SOFCs) and oxygen sensors [1, 2]. Being a fast oxide ion conductor, $\text{La}_2\text{Mo}_2\text{O}_9$ has attracted much interest since its introduction by Lacorre in 2000 [3]. The main advantage of this material is the excellent ionic conductivity for temperatures above 570°C which is comparable to those of the commercialized yttria stabilized zirconia (YSZ) and gadolinium doped ceria (CGO). Although the phase transition (β -phase to α -phase) upon cooling to $\sim 570^\circ\text{C}$ causes a number of negative effects, e.g. the unit cell volume change, the significant drawback is a reduction in its ionic conductivity by almost two orders of magnitude [3]. Many studies have now effectively proved that substituting the La site with Gd [4], Er, Dy, [5] and others [6] can suppress the phase transition and stabilize the conducting β phase. Moreover, substitution of the Mo site with W can also improved the material by increasing its resistance to the reducibility of Mo [7]. These substituted derivatives are referred to as the LAMOX family (the substituted $\text{La}_2\text{Mo}_2\text{O}_9$ materials). Apart from the improvements of the electrical properties, understanding the crystal structure and the oxygen transport mechanism is an essential guide to optimizing these materials and promoting their application [8, 9].

Measurement of the oxygen surface exchange and diffusion coefficients is an excellent method by which the oxygen mobility within a material can be directly determined. From the diffusion coefficient, the number of mobile charge carriers can be calculated and correlated with the measured conductivity. To date the oxygen isotope diffusion measurement has been applied to many electroceramics, such as $\text{La}_{2-x}\text{Sr}_x\text{NiO}_{4-\delta}$ [10], YSZ [11] and CGO [12]. However, there are few oxygen diffusion studies of the LAMOX family [13]. One of the main reasons for this is the difficulty associated with the oxygen exchange process i.e. the low

number of available electrons restricts the charge transfer in the oxygen dissociation on the surface, as shown in the reaction $\text{O}_2 + 4\text{e}^- \rightarrow 2\text{O}^{2-}$ [14]. To overcome this limitation, one solution is to perform the isotope exchange in a humidified atmosphere. It is suggested that the adsorbed water on the surface plays an important role in the oxygen isotope exchange reaction [15, 16] with dissociation of H_2O being more favourable than that of O_2 (g). The only previous report [13] of oxygen ion diffusion in LAMOX, which was undertaken in a wet atmosphere, reveals the diffusion profiles at different temperatures and also gives the diffusion coefficients of oxygen ions. This report did, however, raise questions about the nature of the oxygen transport in LAMOX. To date there have not been, to our knowledge, any reports regarding the oxygen exchange and diffusion using a dry atmosphere for $\text{La}_2\text{Mo}_2\text{O}_9$.

Silver has been noted as a good catalyst for the electrochemical reduction of oxygen in Ag/electrolyte systems [17, 18]. The application of silver to enhance the surface oxygen exchange for diffusion in ionic conductors has already been demonstrated [19]. For ionic conductive materials, the oxygen surface exchange is limited by the availability of electrons which are necessary for the oxygen dissociation [20]. By applying a silver coating to the surface, the dissociation of oxygen molecules may occur on the silver surface. Moreover, the oxygen reduction process may take place easily at the triple phase boundary (TPB) where the dissociated oxygen can directly combine with oxygen vacancies in the electrolyte. By optimising the surface exchange of the electrolyte, a diffusion profile can be obtained from which the diffusion coefficient can be calculated. However, it is important to note that the surface exchange coefficient can no longer reflect the surface reactive property of the electrolyte.

In this paper, we report on the characterization of the oxygen transport in $\text{La}_2\text{Mo}_2\text{O}_9$ under dry conditions using an isotopic labelling technique previously described elsewhere [21]. These studies further demonstrate the fast oxygen ion transport of $\text{La}_2\text{Mo}_2\text{O}_9$ whilst also highlighting the important role a catalyst has, in this particular case silver.

2. Experimental

2.1 Sample preparation

$\text{La}_2\text{Mo}_2\text{O}_9$ powder was prepared by conventional solid state synthesis [4, 7]. The starting materials, La_2O_3 (99.9%, Aldrich) and MoO_3 (99.5%, Aldrich) were mixed stoichiometrically and ball-milled under acetone with stabilized zirconia milling media for 24 hours (La_2O_3 powder was pre-heated at 1000°C for 6 hours before mixing). After being dried, the mixture was heated to 500°C for 12 hours and then to 900°C for a further 24 hours. $\text{La}_2\text{Mo}_2\text{O}_9$ pellets were made by uni-axial pressing followed by iso-static pressing at 300 MPa, and then sintering at 1000°C for 2 hours. The sample density was determined using the Archimedes technique, with all specimens found to be greater (taking account of a standard deviation of 0.2%) than 95% of their theoretical density.

In order to obtain high-quality results using secondary ion mass spectrometry (SIMS), sample preparation followed the method which has been used in previous studies [22, 23]. The dense pellets were polished with diamond slurry down to a finish of $0.25\mu\text{m}$. The polished surface was then coated with silver (100nm, 99.99%) using an Emitech K575X sputter coater (with a magnetron target assembly).

2.2 Oxygen isotope exchange and diffusion measurement

Oxygen diffusion was studied using the isotope exchange technique followed by secondary ion mass spectrometry, as discussed in previous studies [24, 25]. The details of the oxygen exchange apparatus has been described previously [21]. Samples were pre-annealed in dry research grade oxygen (BOC 99.996%) of natural isotopic abundance for a duration of 10 times that of the isotopic exchange time [26] to ensure oxygen equilibration. The equilibrated sample was then annealed in ^{18}O enriched gas at a pressure of 200 mbar for 30 minutes before being rapidly quenched to room temperature. Previously reported [13] ‘wet’ exchange samples had been exposed to an atmosphere of H_2^{18}O at the anneal temperature and subsequently slow cooled to 100°C , leading to a key experimental difference between the data reported here and that of George *et al.*

After the exchange, the diffusion profile was obtained by SIMS. Generally, two different approaches were applied. Starting at the exposed sample surface, depth profiles, measuring the ^{16}O and ^{18}O intensities as a function of sputter time (corresponding to increasing depth) were taken. In cases where the penetration depth of the diffusing species was larger than $100\text{ }\mu\text{m}$, SIMS images or line scans [27] were taken from polished cross sections (polishing down to a finish of $0.25\text{ }\mu\text{m}$). In order to avoid polishing residues influencing the data, a sputter cleaning of the area of analysis was performed prior to analysis.

Two quadropole SIMS instruments (Atomika 6500 with a nitrogen primary ion beam (Department of Materials, Imperial College London) and Atomika 4500, using an Ar^+ primary ion beam (Department of Physics, University of Warwick)) and a TOF-SIMS instrument (TOF-SIMS 5-300, ION TOF operated at Tascon GmbH, Münster, Germany) were used for the measurements. For the Atomika instruments, the incident N_2^+ beam energy was 5 keV

with an ion current of 60nA for the Atomika 6500, while the Ar⁺ beam was 2.5 keV and 75nA for the Atomika 4500. The obtained diffusion profiles were analyzed using Crank's solution to Fick's second law of diffusion. The solution is given as [28]:

$$C_1(x) = \operatorname{erfc}\left(\frac{x}{2\sqrt{D^*t}}\right) - e^{(hx+h^2D^*t)} \operatorname{erfc}\left\{\left(\frac{x}{2\sqrt{D^*t}}\right) + (h\sqrt{D^*t})\right\} \quad (1)$$

where $C_1(x)$ is the normalised isotopic fraction at a depth x and is normalized to the gas concentration, C_g , as shown in Equation 2. D^* is the self-diffusion coefficient, t is the isotopic exchange time and h is the ratio of surface exchange coefficient k to D^* .

$$C_1(x) = \frac{C(x) - C_{bg}}{C_g - C_{bg}} \quad (2)$$

where $C(x)$ is the ratio of $^{18}\text{O}^-$ intensity to the total intensity of ($^{18}\text{O}^- + ^{16}\text{O}^-$), C_{bg} is the background isotopic fraction in the material, and C_g is the isotopic fraction of the exchange gas which is assumed to remain constant throughout the exchange experiment. The length $2(D^*t)^{0.5}$ is commonly called “the diffusion length” and represents the decay of the diffusion concentration with depth.

The TOF-SIMS instrument was operated using Bi_1^+ primary ions at 25 keV energy. Sputtering, either for depth profiles or for surface cleaning, was performed using Cs^+ at 2 keV energy. In contrast to the Atomika instruments depth profiles in the ION-TOF instrument were obtained in the dual beam mode with one primary ion gun (Cs) eroding the surface and a second ion gun (Bi) addressing the respective crater bottom. This approach allows the optimisation of the sputter and analysis conditions independently. Therefore it is possible to achieve information on the lateral and depth distribution of elements with both high lateral and high depth resolution [29].

2.3 Other techniques

X-ray diffraction (XRD) data (30 s/step, $2\theta=20^\circ\sim80^\circ$, $\Delta(2\theta)=0.02^\circ$) were obtained to check the phase purity of the as-prepared materials and also to check if there was any reaction between the sample and the surface coating after the exchange process. A Philips PW 1700 series instrument with CuK_α radiation operating at 40 kV/40mA was used in this study. Scanning electron microscopy (SEM) (JEOL JSM 5610 LV, Japan) and a focused ion beam (FIB) (FEI FIB200) were used to image the silver coated surface after the isotopic exchange and the section of a silver droplet located at grain boundaries.

3. Results and Discussion

3.1 Diffusion profiles and analysis

The diffusion profiles of the samples that were isotope exchanged at their intended temperatures of 450, 500, 550, 600, 650 and 700°C are shown in Fig. 1. The measured temperatures obtained from a thermocouple located beside the sample are also listed in Table 1. It is apparent that the oxygen diffusion length increases with increasing isotopic exchange temperature, especially above 600°C where the expansion of the $\text{La}_2\text{Mo}_2\text{O}_9$ unit cell releases more space for oxygen transport [30]. Moreover, it is clear that the Ag coating has enhanced the surface exchange and thus helped to obtain the oxygen diffusion profiles even at low temperature [13].

Georges *et al.* [13] have reported an elongated tail in the wet exchange diffusion profile and therefore applied the Le Claire solution [31] to their fitting to incorporate a tailing function. Although there were two possible explanations for this tailing behaviour, based on the consistency between the fitting and the profile, the presence of grain boundary diffusion was suggested. However, in our work, the dry exchange diffusion profiles at all temperatures fitted extremely well to the Crank solution and therefore no tailing correction to the fit was required.

The difference in the diffusion behaviour of $\text{La}_2\text{Mo}_2\text{O}_9$ implies that the previously reported tailing behaviour could be an experimental artefact as a result of the slow cooling procedure used in the wet exchange process, while in the current study sample quenching was applied to minimize the effect of diffusion during cooling. The intrinsic diffusion coefficient at the anneal temperature will not be affected by this difference in exchange procedure, but with a slow cooling process the intrinsic kinetic parameters are not obtained, as discussed by Vannier et al [23]. The previously reported ‘wet’ exchange diffusion coefficients may therefore be a summation of diffusion coefficients at a number of temperatures, resulting in tailing behaviour. We also note that the synthesis and processing method detailed by Georges *et al.* [13] in a previous publication and ourselves is nominally the same and therefore the possibility of the effects of microstructure on the diffusion can be eliminated. However, these potential differences between the dry and wet exchanges e.g. the existence of the grain boundary diffusion in the wet exchange, requires further work. It is clear that under dry conditions, no tailing was observed in this series of samples.

The measured diffusion and surface exchange coefficients are listed in Table 1. Because of the surface modification introduced by the silver coating, the obtained surface exchange coefficient, k , deduced from the fitting of the diffusion profile using the non-linear least square equation, is not characteristic of the $\text{La}_2\text{Mo}_2\text{O}_9$ surface. A dimensionless parameter $h' = k(t/D)^{0.5}$ is introduced to indicate the level of confidence in the estimation of D^* and k . Ideally, the diffusion anneal should be tailored to give h' values in the range of 0.1~4.0 so that the obtained diffusion profiles can yield reliable values of both D^* and k [24]. The low value of h' , in our case, is a result of the small surface concentration, which is often found in fast oxygen ion conductors where surface exchange is slow in comparison with diffusion. The fact that h' is less than 0.1 indicates that the confidence in the D^* measurement could be reduced

[25]. The diffusion coefficients are also plotted in Fig. 2 along with the previously reported diffusion coefficients as a comparison. There is an obvious jump of about one order of magnitude in the diffusion coefficient values when the exchange temperature was increased from 550°C to 600°C which coincides with the temperature range for the α - β phase transition. The previously reported diffusion coefficients are higher than those obtained in this work, which might be a result of chemical differences between the materials. However, the data trend suggests a significant difference between the activation energy for the two data sets. For the data points within the temperature range 600-700°C, the activation energy is found to be 0.66(\pm 0.09) eV, while for the low temperature range (450-550°C) it is 1.25(\pm 0.01) eV. The activation energy reported in the literature [13] for the high temperature data was 1.11(\pm 0.16)eV significantly larger than the value found here. No other literature data are available for a comparison of the activation energies in the low temperature regime. This difference in the activation energy may reflect the differences between the two exchange methods. As the silver coating is not expected to have any effect on the bulk diffusion coefficient, it is more likely that the wet exchange method has led to a variation in the diffusion coefficient measurement leading to the higher activation energy reported for oxygen diffusion, possibly due to the effect of slow cooling of the labelled samples prior to analysis. Moreover, the lower activation energy at high temperature indicates a lower energy barrier for oxygen transport, which is consistent with the increase of the conductivity due to the open crystal structure of β -La₂Mo₂O₉ after the phase transition [30].

As reported previously [12], the oxygen exchange and diffusion was interpreted as a three step process: (1) oxygen adsorption on the surface; (2) oxygen dissociation which involves charge transfer; (3) oxygen incorporation via oxygen vacancies in the electrolyte. Of these three steps, the oxygen dissociation is commonly considered as the rate-determining step

because of the difficulty of charge transfer in ceramics [21]. The silver film applied acts as a catalyst for the oxygen dissociation and also increases the number of triple phase boundaries (TPBs) that facilitate charge transfer. However, in the samples which were exchanged at higher temperatures, 795, 848 and 893°C, the surface isotopic concentration was so low that we could not obtain the diffusion coefficients by fitting to the experimental profiles, as shown in Fig. 3. We believe that the ^{18}O exchange at these elevated temperatures was surface limited, suggesting that the silver coating on the surface might have degraded in some way, thus reducing the surface exchange kinetics.

3.2 Stability of the silver coating

As mentioned previously, we believe that for the high exchange temperatures used here, the catalyst coating was deactivated through the loss of silver (e.g. evaporation) or a chemical reaction of the Ag coating with $\text{La}_2\text{Mo}_2\text{O}_9$. XRD patterns were obtained to investigate the surface of the samples (Fig. 4). From the XRD it is clear that at low temperature, the surface silver coating remained intact (Fig. 4 (a)), while there was little silver left after the sample was exchange annealed at the higher temperature ($\geq 800^\circ\text{C}$) (Fig. 4 (b)). This corresponds well with the diffusion profiles found for the low ($\leq 700^\circ\text{C}$) and high temperatures ($\geq 800^\circ\text{C}$). There were no impurity peaks found in both XRD diffraction patterns, indicating that the silver was chemically stable on $\text{La}_2\text{Mo}_2\text{O}_9$ despite the relatively high anneal temperature of about 800°C . However, taking into consideration the resolution of the XRD technique, we have to leave the question open as to whether there is any amalgam i.e. Ag/(La or Mo), reactivity between Ag and $\text{La}_2\text{Mo}_2\text{O}_9$ or amorphous silver on the surface.

The agglomeration of silver as a function of temperature has been studied before [32, 33] where the silver was found to redistribute itself and form a network of “islands” at low

temperature. For increasing temperatures, especially under low pressure, the silver film goes through a series of changes, such as evaporation, or even sublimation [34]. To observe the silver morphology on the exchanged samples, SEM was used to image the surfaces.

In Fig. 5 (a) and (b), we see that after the sample was heat-treated at about 500°C and 700°C, the silver formed a network of “islands” on the surface. A possible reason for this is to minimize the surface energy of the ceramics [35] because of its non-wetting behaviour. This type of silver network will have played a positive role in the oxygen surface exchange due to the enlarged TPB area where electrolyte, oxygen gas and silver regions contact. However, for high temperatures such as 893°C, Fig. 5 (c), the island coverage became smaller and the distribution changed into a regular pattern along the grain boundaries. This decreased coverage would explain the low surface concentration of ^{18}O observed in the samples annealed at higher temperatures. The FIB technique [36] was applied to investigate a section of a silver particle at the grain boundary. The result (inset of Fig. 5) appears to exclude the possibility of the silver particles diffusing into the grain boundaries, which means the loss of silver at elevated temperature is likely to be a result of silver evaporating from the surface.

3.3 Oxygen isotope tracer surface distribution

For the sample exchanged at 698°C, 3D TOF-SIMS depth profiles were acquired in order to investigate the influence of silver on the oxygen exchange and its distribution in the near surface layers.

Sputtering was performed over an area of $300 \times 300 \mu\text{m}^2$ using a current of 120 nA. Imaging of the crater center ($100 \times 100 \mu\text{m}^2$) was performed using a Bi_1^+ beam at a current of 0.05 pA in burst mode (allowing simultaneously high mass and lateral resolution). Results are presented

in Fig. 6. The track within the selected area (Fig. 6(a)) is believed to be a scratch on the surface, and the reason for choosing this area is that the silver coating was damaged during the sample preparation after the exchange, therefore the silver islands are more likely to remain untouched within the track, making this a useful region for studying the relationship between oxygen and the silver coating.

In Fig. 6(b), the LaO_2^+ and MoO_2^+ images show a uniform lateral surface element distribution and thus confirm the homogeneity of the prepared $\text{La}_2\text{Mo}_2\text{O}_9$ sample. Carbon, chlorine, and phosphorus contamination are evident from these maps the origin of which is currently being sought. Of significance is the strong relationship between ^{18}O and Ag. Despite the damage to the silver coating during polishing, the positions of the silver particles left in the track are consistent with the ^{18}O enriched area. This phenomenon was confirmed by correlation analysis (3-colour-overlay) of three TOF-SIMS maps representing the Ag, ^{18}O and C distribution. Carbon is mostly located in the open pores on the surface.

From the 3D data stream the depth profiles of ^{18}O and ^{16}O can be retrieved for both the ^{18}O enriched and the less enriched areas (Fig. 7). The depth profiles show that in the ^{18}O enriched area (the area with Ag), the ^{18}O concentration is twice as high as that where less Ag was present. This relatively high concentration could be associated with dissolved oxygen in the silver [37], but it could also be related to the improved oxygen exchange on the ceramic surface.

3D depth profiling has therefore identified some issues regarding the isotopic exchange of $\text{La}_2\text{Mo}_2\text{O}_9$ in the near surface layers. On a larger scale, however, the element mapping results for ^{16}O and ^{18}O over an area of $500 \times 500 \mu\text{m}^2$ of a cross section of the sample exhibits

satisfactory uniform oxygen diffusion along the depth direction, as shown in Fig. 8. From these data, the obtained diffusion coefficient was determined to be $4.7 \times 10^{-7} \text{ cm}^2 \cdot \text{s}^{-1}$, which agrees well with the value already determined from the line scan technique on other instruments as listed in Table 1 and therefore reaffirms the validity of the obtained diffusion coefficients. This also indicates that the surface oxygen incorporation enhancement involving the Ag catalysis did not have a significant effect on the diffusion profile.

4. Conclusion

We have shown that a silver coating has a significant influence on the surface oxygen exchange properties of $\text{La}_2\text{Mo}_2\text{O}_9$. It was shown that a thin silver film enhances the surface oxygen dissociation and thus improves the surface exchange coefficient. Therefore, diffusion profiles can be obtained for ionic conductors enabling the diffusion coefficient for such electrolyte materials to be obtained. However, because of the silver layer instability at high temperature ($>700^\circ\text{C}$), all attempts to obtain the diffusion profiles at these high temperatures were unsuccessful. The diffusion profiles obtained for the temperatures lower than 700°C did show some differences compared with those previously published [13] which involved a grain boundary diffusion effect, suggesting that in dry conditions there is no significant grain boundary diffusion for the $\text{La}_2\text{Mo}_2\text{O}_9$ material. The difference in the activation energy between our work and the previous report [13] might suggest the isotopic exchange atmosphere has some effects on the oxygen diffusion in $\text{La}_2\text{Mo}_2\text{O}_9$.

Morphology studies of the silver on the surface showed that for an increasing exchange temperature, the silver coating underwent a series of changes, from a network of silver

“islands” at low temperature ($\leq 700^\circ\text{C}$) to a severely damaged silver coating at high temperatures ($> 700^\circ\text{C}$). Surface analysis using TOF-SIMS indicated that the oxygen dissociation and exchange were not uniform while there was a correlation found between the formed silver islands and where the sample was ^{18}O enhanced. Although the diffusion profile extracted from the element mapping showed silver distribution and the un-uniform oxygen incorporation on the surface did not appear to have a significant effect on the diffusion profile, the mechanism behind the surface reaction during exchange still requires further investigation.

Based on these results, further work regarding the silver coating on the diffusion and surface exchange of the $\text{La}_2\text{Mo}_2\text{O}_9$ ionic conductor are under way.

5. Acknowledgements

The authors would like to thank the Lee Family for funding a studentship (J. Liu). The authors also wish to thank Elke Tallarek (Tascon GmbH, Münster, Germany) for performing the TOF-SIMS analysis and are grateful to ION-TOF GmbH, Münster, Germany, for enabling the data collection by TOF-SIMS.

References

1. Skinner S. J., Kilner J. A., *Materials Today*, 2003, 3: 30-37.
2. Marques F. M. B., Kharton V. V., Naumovich E. N., *Solid State Ionics*, 2006, 177(19-25): 1697-1703
3. Lacorre P., Goutenoire F., Bohnke O., *Nature*, 2000, 404: 856-858.
4. Georges S., Goutenoire F., Altorfer F., Sheptyakov D., Fauth F., Suard E., Lacorre P., *Solid State Ionics*, 2003, 161(3-4): 231-241.
5. Tsai D. S., Hsieh M. J., Tseng J. C., Lee H. Y., *J. Eur. Ceram. Soc.*, 2005, 25(4): 481-487.
6. Marrero-Lopez D., Perez-Coll D., Ruiz-Morales J. C., Canales-Vazquez J., Martin-Sedeno M. C., Nunez P., *Electrochim. Acta*, 2007, 52: 5219-5231.
7. Georges S., Bohnke O., Goutenoire F., Laligant Y., Fouletier J., Lacorre P., *Solid State Ionics*, 2006, 177: 1715-1720.
8. Goutenoire F., Isnard O., Retoux R., Lacorre P., *Chem. Mater.*, 2000, 12(9): 2575-2580.
9. Evans I. R., Howard J. A. K., Evans J. S. O., *Chem. Mater.*, 2005, 17(16): 4074-4077.
10. Skinner S. J., Kilner J. A., *Solid State Ionics*, 2000, 135: 709-712.
11. De Souza R. A., Pietrowski M. J., Anselmi-Tamburini U., Kim S., Munir Z. A., Martin M., *Phys. Chem. Chem. Phys.*, 2008(10): 2067-2072.
12. Lane J. A., Kilner J. A., *Solid State Ionics*, 2000, 136-137: 927-932.
13. Georges S., Skinner S. J., Lacorre P., Steil M. C., *Dalton Trans.*, 2004(19): 3101-3105.
14. Boukamp B. A., Van Hassel B. A., Vinke I. C., De Vries K. J., Burggruf A. J., *Electrochim. Acta*, 1993, 38(14): 1817-1825.
15. Sakai N., Yamaji K., Horita T., *J. Electrochem. Soc.*, 2003, 150(6): A689-A694.

16. Sakai N., Yamaji K., Negishi H., Horita T., Yokokawa H., Xiong Y. P., Phillipps M. B., *Electrochemistry*, 2000, 68(6): 499-503.
17. Wang J. H., Liu M. L., C. L. M., *Solid State Ionics*, 2006, 177: 939-947.
18. Van Herle J., McEvoy A. J., *J. Phys. Chem. Solids*, 1994, 55(4): 339-347.
19. Raj E. S., Atkinson A., Kilner J. A. 8th European Solid Oxide Fuel Cell Forum. Lucerne, Switzerland.2008 : A0714.
20. Ji Y., Kilner J. A., Carolan M. F., *Solid State Ionics*, 2005, 176: 937-943.
21. Manning P. S., Sirman J. D., Kilner J. A., *Solid State Ionics*, 1997, 93: 125-132.
22. Kilner J. A., Steele B. C. H., *Solid State Ionics*, 1984, 12: 89-97.
23. Vannier R. N., Skinner S. J., Chater R. J., Kilner J. A., Mairesse G., *Solid State Ionics*, 2003, 160: 85-92.
24. Kilner J. A., De Souza R. A., *International Symposium on Materials Science: high temperature electrochemistry-ceramics and metals*, Denmark, 1996 : 41-54
25. Atkinson A., Chater R. J., Rudkin R., *Solid State Ionics*, 2001, 139: 233-240.
26. De Souza R. A., Kilner J. A., *Solid State Ionics*, 1998, 106: 175-187.
27. Chater R. J., Carter S., Kilner J. A., Steele B. C. H., *Solid State Ionics*, 1992, 53-56: 859-867.
28. Crank J., *The mathematics of diffusion*. 1975, Oxford: Oxford University Press.
29. <http://www.ion-tof.com/technique-sims-IONTOF-TOF-SIMS-TIME-OF-FLIGHT-SURFACE-ANALYSIS.htm>. (accessed: 20/09/2009)
30. Tealdi C., Malavasi L., Ritter C., Flor G., Costa G., *J. Solid State Chem.*, 2008, 181: 603-610.
31. Harries I. R., Jones I. P., *Grain Boundaries: Their Character, Characterisation and Influence on Properties*. 2001: Maney Publishing.
32. Kim H. C., Alford T. L., *Applied Physics Letters*, 2002, 81(22): 4287-4289.

33. Alford T. L., Chen L. H., Gadre K. S., Thin Solid Films, 2003, 429(1-2): 248-254.
34. Dushman S., Lafferty J. M., *Scientific Foundations of Vacuum Technique*. 1966: John Wiley & Sons Inc.
35. Simrick N. J., Kilner J. A., Atkinson A., 8th European Solid Oxide Fuel Cell Forum Lucerne, Switzerland.2008 : A0608.
36. Phaneuf M. W., Micron, 1999, 30 : 277-288
37. Adler S. B., Chem. Rev., 2004, 104: 4791-4843.

List of Table Captions

Table 1. Experimental details and kinetic parameters determined from $\text{La}_2\text{Mo}_2\text{O}_9$ samples as a function of temperature. The value of h' is included as a reliability factor.

Table List

Table 1

Exchange Temp (°C) Intended / Measured	Exchange Time (s)	D* (cm ² s ⁻¹)	k (cm s ⁻¹)	h' (=k(t/D) ^{0.5})
450 / 447	1810	4.8×10 ⁻¹⁰	3.1×10 ⁻⁸	0.060
		4.9×10 ⁻¹⁰	2.9×10 ⁻⁸	0.056
450 / 459	2400	5.2×10 ⁻¹⁰	2.3×10 ⁻⁸	0.049
		4.8×10 ⁻¹⁰	2.6×10 ⁻⁸	0.058
		7.5×10 ⁻¹⁰	4.6×10 ⁻⁸	0.082
		7.0×10 ⁻¹⁰	5.2×10 ⁻⁸	0.096
500 / 500	1200	1.6×10 ⁻⁹	4.8×10 ⁻⁸	0.042
		1.4×10 ⁻⁹	5.5×10 ⁻⁸	0.051
500 / 502	1800	1.4×10 ⁻⁹	7.3×10 ⁻⁸	0.083
		1.4×10 ⁻⁹	4.6×10 ⁻⁸	0.052
		1.8×10 ⁻⁹	8.1×10 ⁻⁸	0.081
		2.7×10 ⁻⁹	1.2×10 ⁻⁷	0.098
		1.2×10 ⁻⁹	7.8×10 ⁻⁸	0.096
		1.0×10 ⁻⁹	5.5×10 ⁻⁸	0.074
550 / 550	1200	6.0×10 ⁻⁹	2.8×10 ⁻⁷	0.125
		6.1×10 ⁻⁹	3.0×10 ⁻⁷	0.133
600 / 596	1200	6.7×10 ⁻⁸	7.9×10 ⁻⁷	0.106
		1.6×10 ⁻⁷	7.1×10 ⁻⁷	0.062
650 / 651	1827	2.1×10 ⁻⁷	4.2×10 ⁻⁷	0.039
		2.1×10 ⁻⁷	4.4×10 ⁻⁷	0.041
		1.9×10 ⁻⁷	4.1×10 ⁻⁷	0.040
700 / 698	1800	2.4×10 ⁻⁷	2.4×10 ⁻⁷	0.021
		2.6×10 ⁻⁷	8.1×10 ⁻⁷	0.068
		4.0×10 ⁻⁷	7.8×10 ⁻⁷	0.052

* Note: k is the surface exchange coefficient for the La₂Mo₂O₉ surface modified by the silver coating. Hence h' is shown only to indicate the reliability in the estimation of both D and k .

List of Figure Captions

Fig. 1. The diffusion profiles recorded at different exchange temperatures with the fitting results displayed as solid lines.

Fig. 2 Arrhenius plot of the diffusion coefficients for the prepared $\text{La}_2\text{Mo}_2\text{O}_9$, with the previously reported values as a comparison [16]. 10% error bar was added to reflect the accuracy in the determination of D^* in each line scan [24].

Fig. 3 The diffusion profiles of $\text{La}_2\text{Mo}_2\text{O}_9$ recorded after exchange at 795, 848 and 893°C

Fig. 4 XRD pattern of the isotopic exchanged samples with silver coating, with the silver XRD diffraction lines indicated in red. (a) sample exchanged at 550°C; (b) sample exchanged at 848°C

Fig. 5 The images ($125 \times 95 \mu\text{m}^2$) of the silver-coated surface after the exchange at (a) 502 (b) 698 and (c) 893°C (the inset is the section image of a silver particle along the grain boundary using FIB).

Fig. 6 TOF-SIMS data of a sample exchanged at 698°C (a) optical image of the selected area for 3D depth profiling; (b) corresponding secondary ion images; (c) correlation analysis (3-colour-overlay) of Ag, ^{18}O and carbon.

Fig. 7 Depth (sputter time) profiles of the oxygen isotope ratio in ^{18}O enriched areas compared with the ratio in the poorly enriched areas (data taken from the raw data stream of the experiment of Fig. 6)

Fig. 8 TOF-SIMS images of a cross section of an isotopically enriched sample annealed at 698°C (a) ^{16}O mapping image; (b) ^{18}O mapping image; (c) line profiles of ^{16}O and ^{18}O generated by summing up the intensity of all line scans in the chosen area in the mapping.

Figure List

Fig. 1

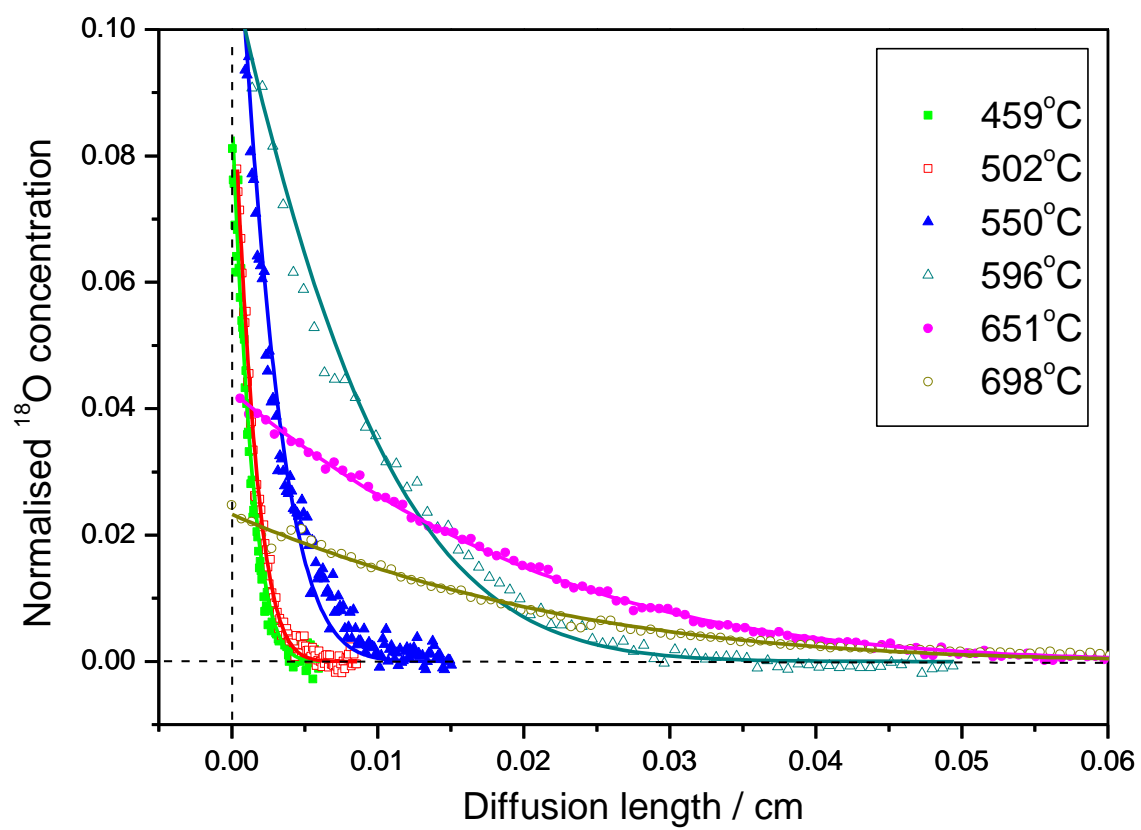


Fig. 2

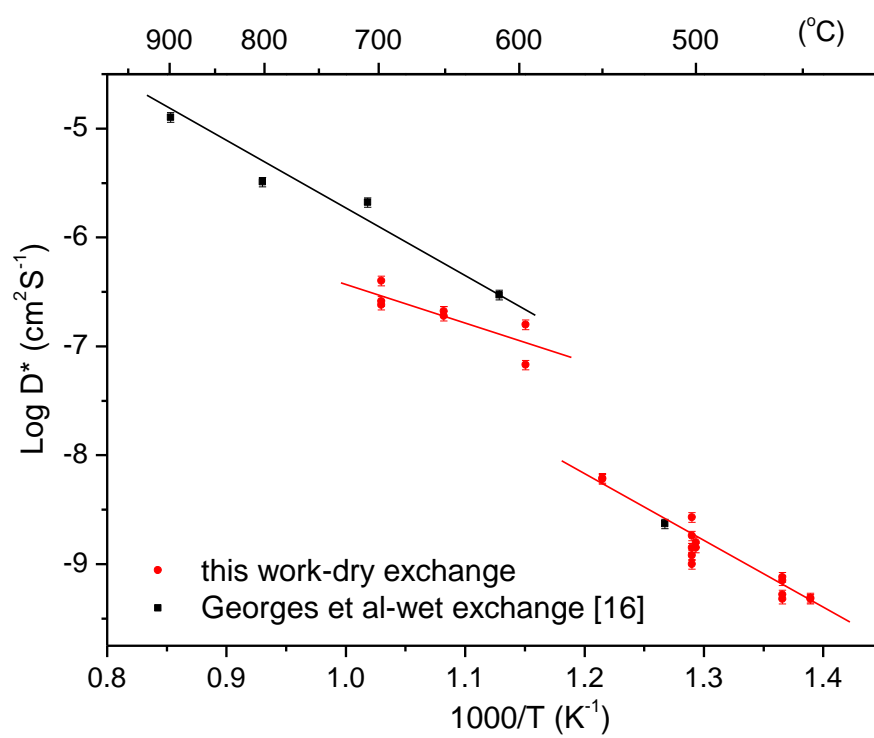


Fig. 3

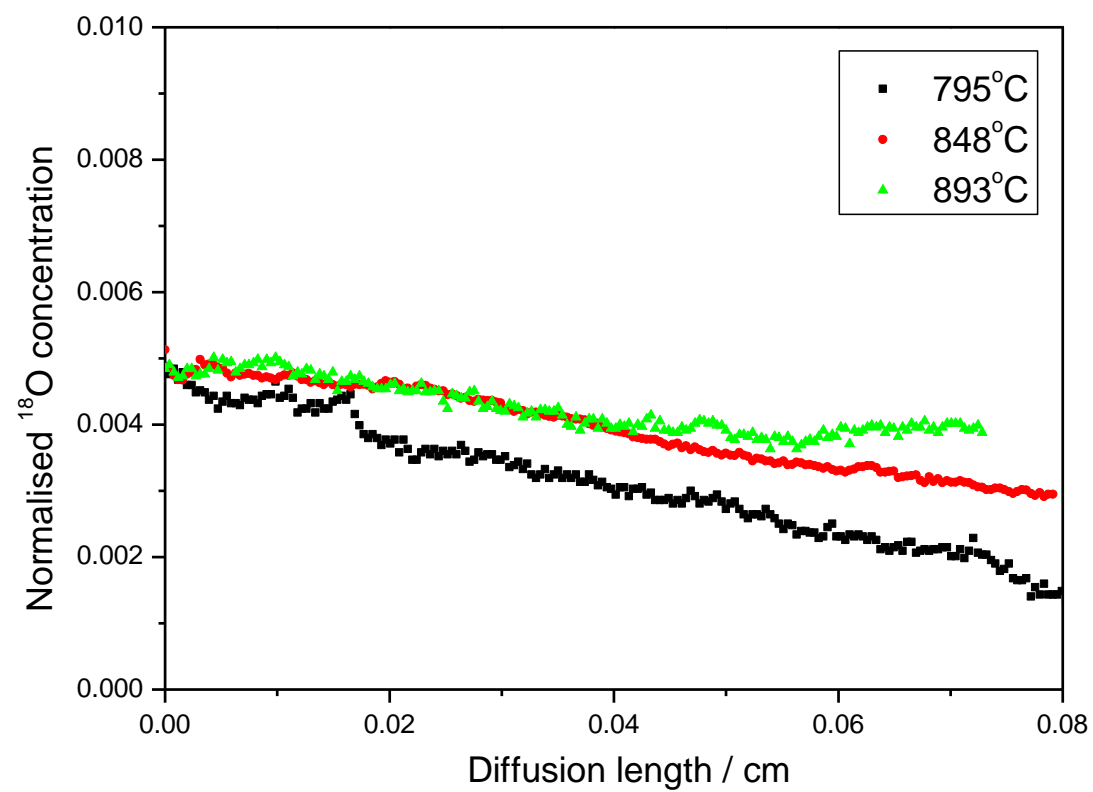
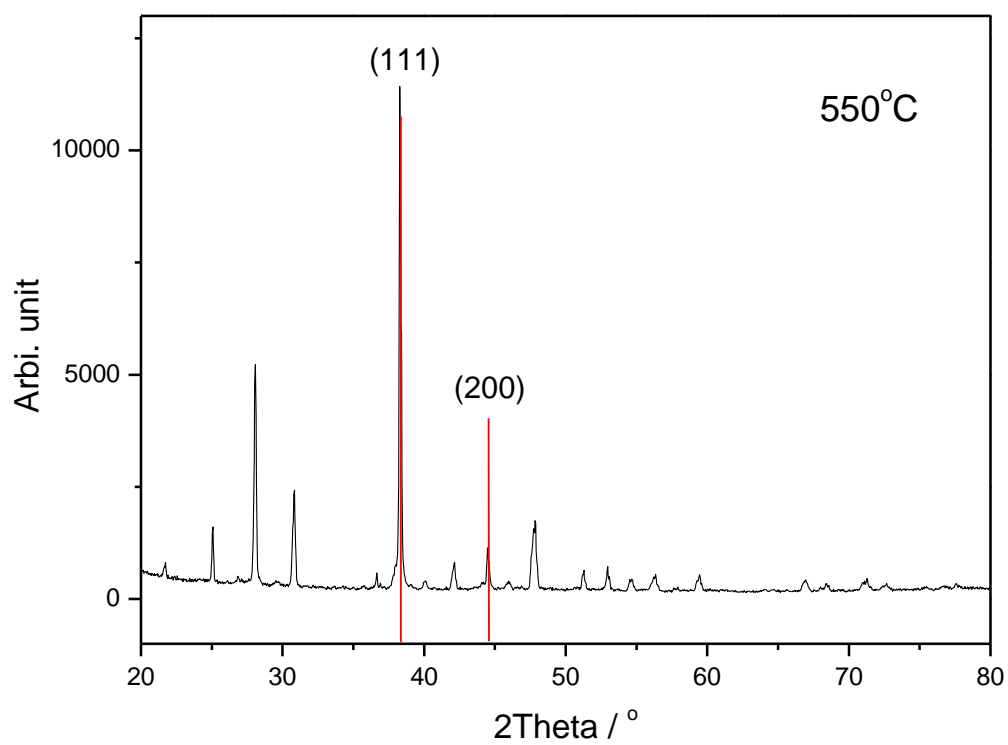
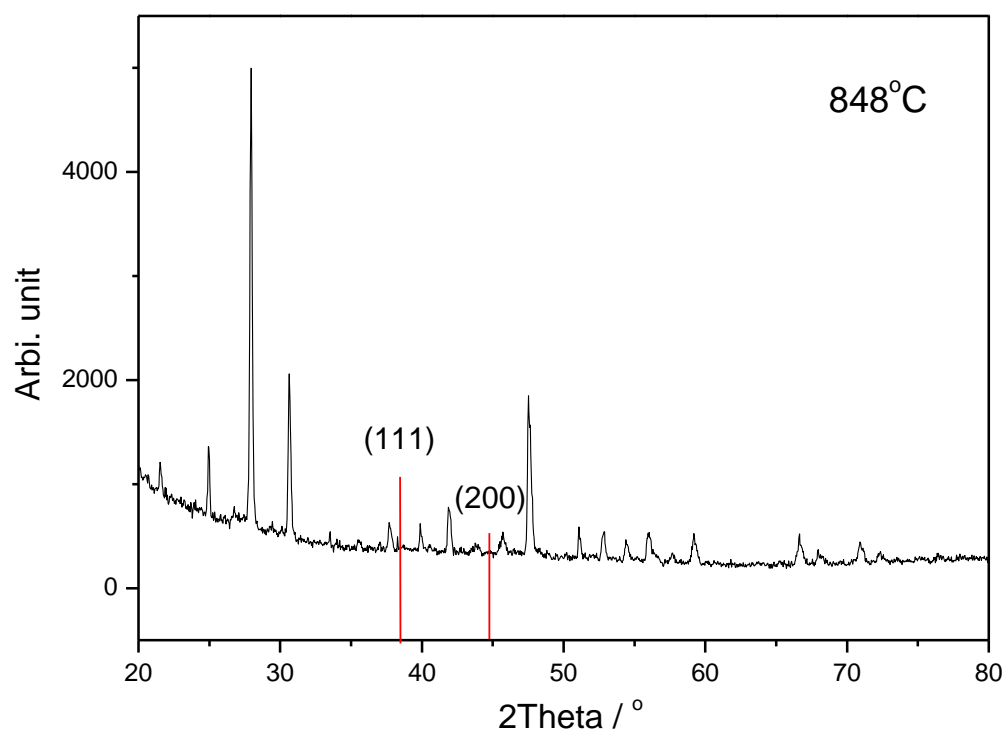


Fig. 4

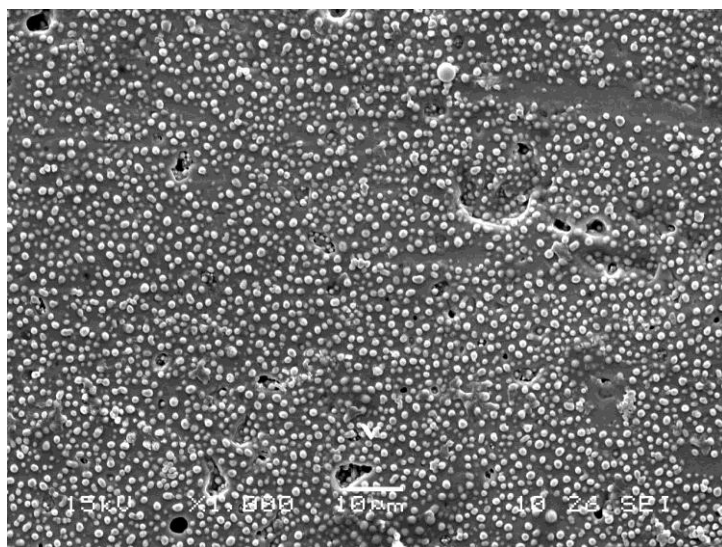


(a)

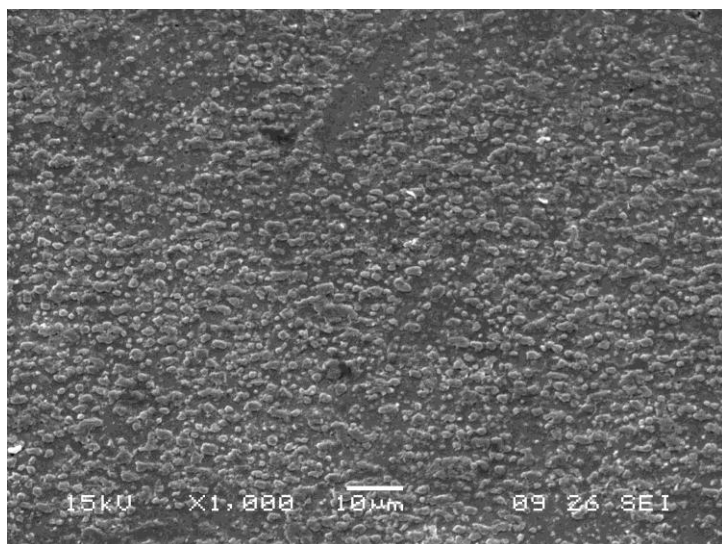


(b)

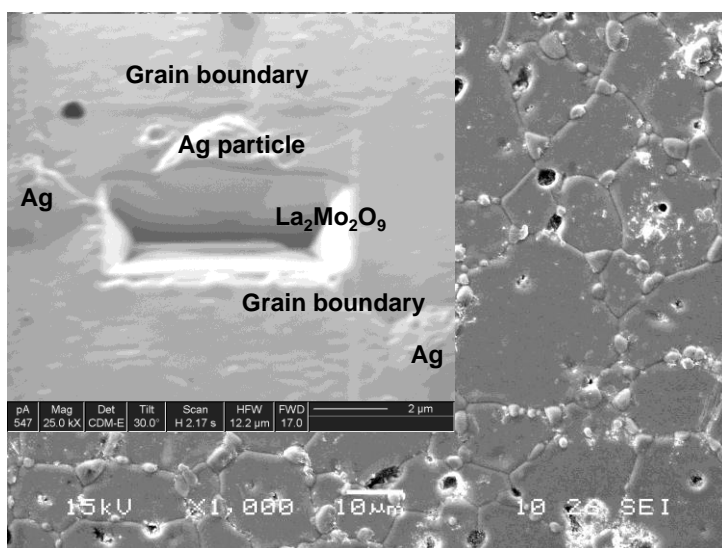
Fig. 5



(a) 502°C



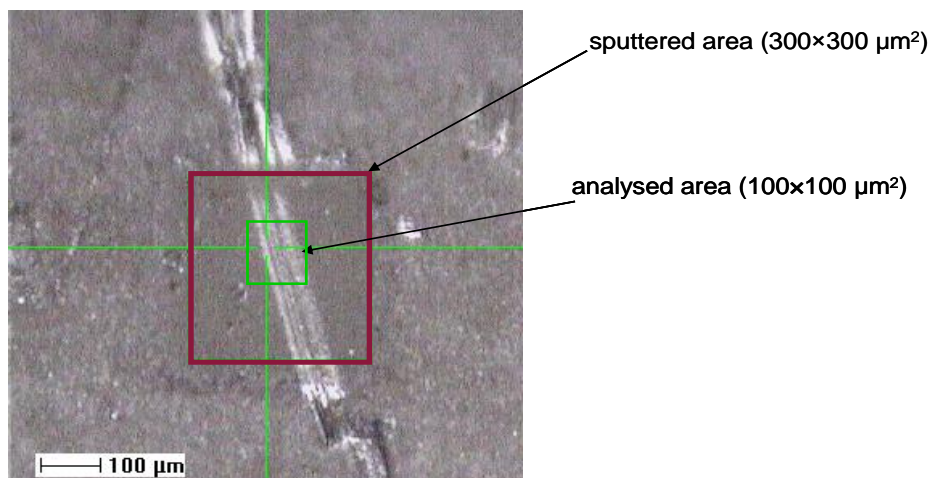
(b) 698°C



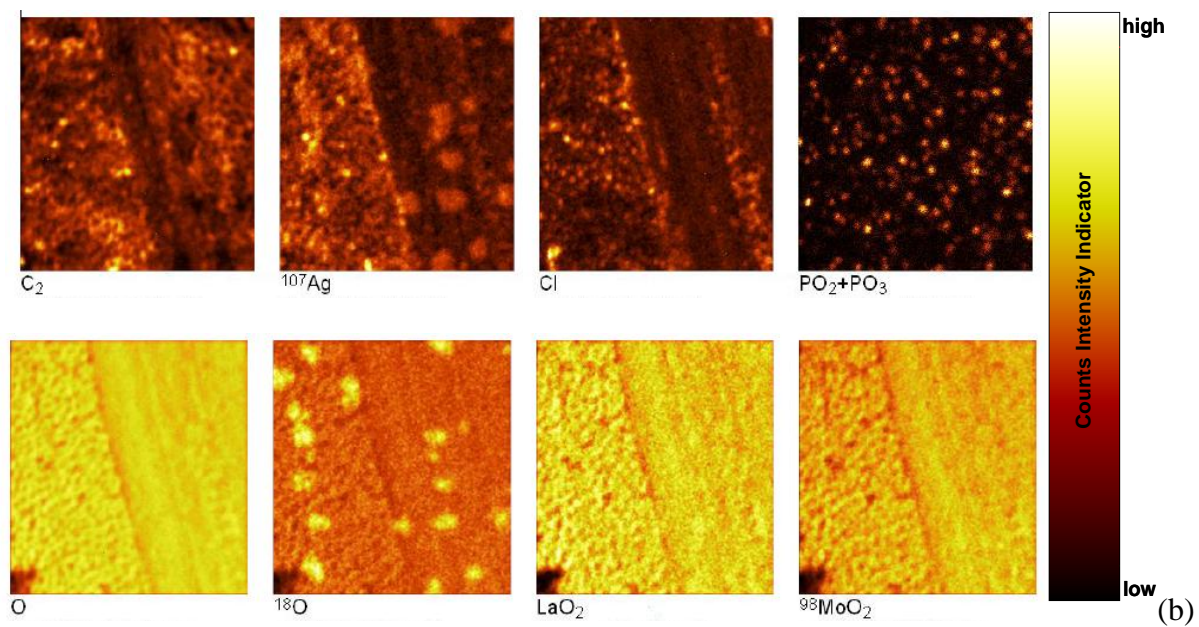
(c) 893°C

Fig. 6

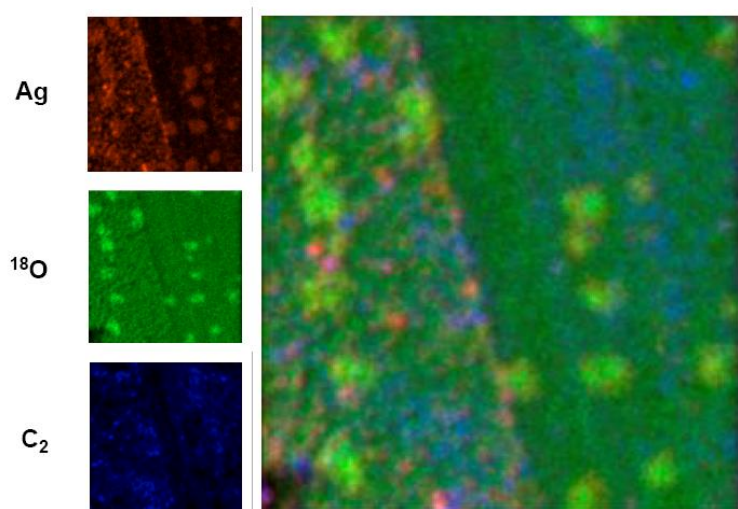
Field of View: $\sim 750 \times 850 \mu\text{m}^2$



(a)



(b)



(c)

Fig. 7

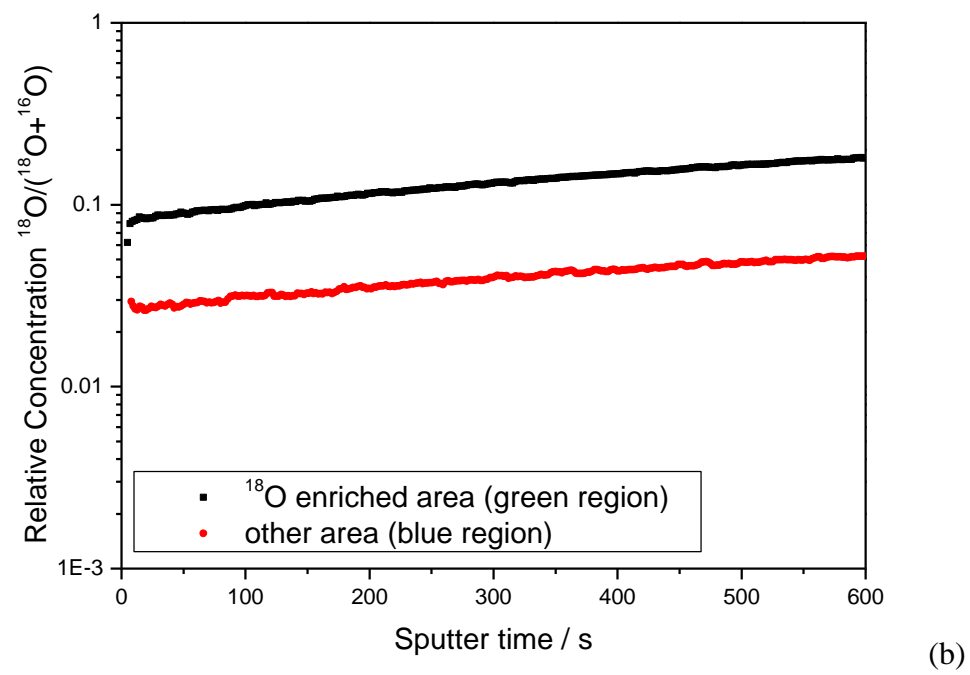
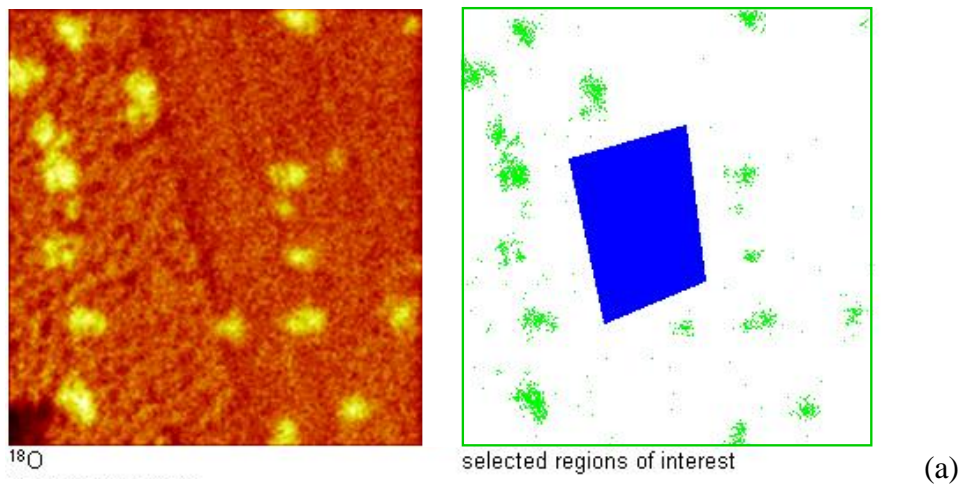


Fig. 8

field of view: 500 x 500 μm^2

